Annals of Nuclear Medicine
https://doi.org/10.1007/s12149-022-01791-z

ORIGINAL ARTICLE

Development of a novel small-animal myocardial phantom can evaluate the image quality of dual-isotope simultaneous acquisition (DISA)

Takayuki Shibutani[1,2] · Masahisa Onoguchi[1,2] · Takayuki Kanno[2,3,4] · Hiroshi Wakabayashi[5] · Tomo Hiromasa[5] · Seigo Kinuya[5]

Received: 22 April 2022 / Accepted: 27 September 2022

Abstract

Background Myocardial phantom studies are widely used as a tool to accurately assess the physical phenomenon of dual-isotope simultaneous acquisition (DISA) in the small-animal fields. However, the previous phantom did not reproduce the structures of rats or mice. The aim of this study was to develop a novel myocardial phantom simulating the structure of a small animal that can be evaluated using the image quality of DISA.

Methods A novel small-animal myocardial phantom that simulated a rat was constructed by the myocardium, liver, lung, spine, and torso. Normal and inferior wall defect myocardial phantoms were filled with ^{99m}Tc or ^{18}F solution to simulate single-isotope acquisition (SIA) and DISA. Phantom and small-animal images with no scatter correction (nonSC) and scatter correction (SC) were created.

Results The ^{99m}Tc DISA with SC showed a low %CV compared to that with nonSC. Although the ^{99m}Tc DISA with nonSC had lower cavity contrast than that of ^{99m}Tc SIA with nonSC, the cavity contrast of SC had similar values between SIA and DISA. The minimum %uptake of ^{99m}Tc SIA with nonSC was a lower value compared to that of ^{99m}Tc DISA with nonSC. The ^{99m}Tc DISA was equivalent to the minimum %uptake of ^{99m}Tc SIA by SC.

Conclusion We have developed a novel myocardial phantom for the rat model to evaluate the image quality for reproducing the physical phenomenon associated with radiation attenuation and scattering. Furthermore, we could demonstrate the usefulness of the novel small-animal myocardial phantom by image quality evaluation of DISA with ^{99m}Tc and ^{18}F compared to SIA.

Keywords Small-animal phantom · DISA · Nuclear cardiology · Mismatch model

Introduction

Molecular imaging such as computed tomography (CT), magnetic resonance imaging (MRI), single-photon emission computed tomography (SPECT) and positron emission tomography (PET) in the cardiovascular field has been widely used in pre-clinical studies because it can provide in vivo information noninvasively [1]. In particular, SPECT and PET imaging enable dynamic imaging of the distribution in vivo to visualize functional information such as blood flow and metabolism, and these images are used to prove the development of new radiopharmaceuticals and the effects of therapeutic agents in pre-clinical studies [2–4]. Many researchers have performed pre-clinical studies using small-animal SPECT or PET devices, which have been evaluated visually and quantitatively [5–10]. Quantitative values in nuclear medicine are useful

✉ Masahisa Onoguchi
onoguchi@staff.kanazawa-u.ac.jp

1 Department of Quantum Medical Technology, Institute of Medical, Pharmaceutical and Health Sciences, Kanazawa University, 5-11-80, Kodatsuno, Kanazawa, Japan

2 Department of Quantum Medical Technology, Graduate School of Medical Sciences, Kanazawa University, Kanazawa, Japan

3 Graduate School of Medicine, Dentistry and Pharmaceutical Sciences, Okayama University, Okayama, Japan

4 Department of Radiological Technology, Nagoya University Hospital, Nagoya, Japan

5 Department of Nuclear Medicine, Kanazawa University Hospital, Kanazawa, Japan

Published online: 13 October 2022

tools for identifying and detecting cardiovascular disease and judging the effects of treatment. On the other hand, the quantitative value in nuclear cardiology is impacted by equipment performance, collimator choice, and the differences in acquisition and image reconstruction methods by each SPECT and PET scanner [11–15]. Therefore, it is important to understand the characteristics of the equipment and image reconstruction to evaluate the quantitative values.

The VECTor^{+}/CT SPECT-PET/CT system (MILabs B.V., Utrecht, Netherlands) is one of the pre-clinical SPECT and/or PET systems, and it realizes simultaneous acquisition of SPECT and PET using clustered-pinhole collimator as opposed to the other devices [11, 16]. The dual-isotope simultaneous acquisition (DISA) has many advantages such as appropriate quantitative evaluation, anatomical registration, the reduction of experimental time and animal welfare owing to the absence of time-phase differences [17–19]. However, the image quality of DISA is affected by physical phenomenon such as scatter and crosstalk depending on the choice of radionuclide. Therefore, we must be properly comprehended the characteristics of DISA.

Myocardial phantom studies are a tool to accurately assess the physical phenomenon such as scatter, radiation attenuation and crosstalk of DISA. Several studies using small-animal myocardial phantoms have already been reported [7, 20, 21]. However, these phantoms did not reproduce the structure of the rat and mice. The aim of this study was to develop a novel myocardial phantom simulating the structure of a small animal that can be evaluated the image quality of SPECT and PET images.

Material and methods

Myocardial phantom

A novel small-animal myocardial phantom that simulated a rat was constructed by myocardium, liver, lung, spine, and torso (Fig. 1). The torso was composed of a cylindrical shape

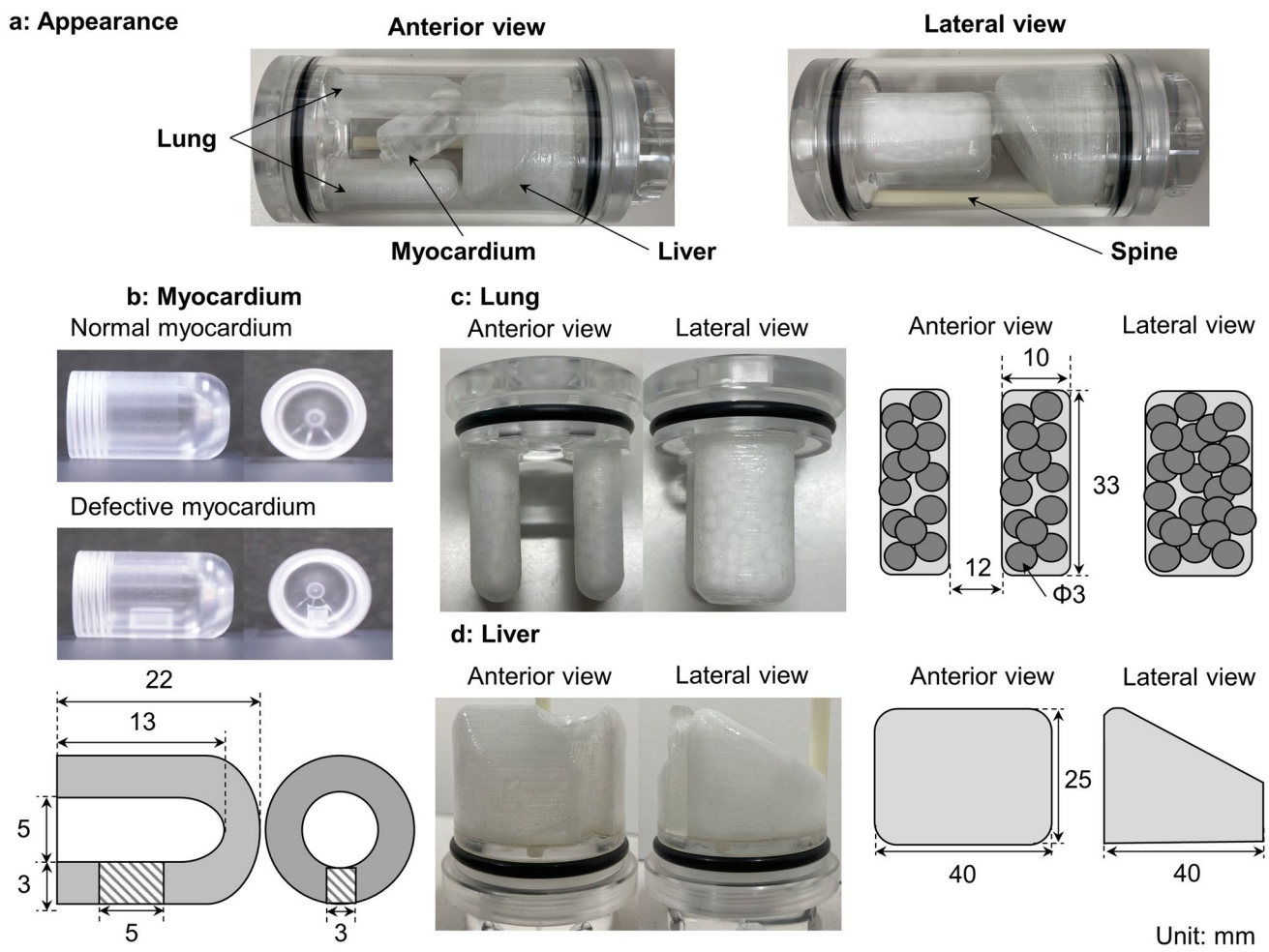

Fig. 1 An overview of a novel small-animal myocardial phantom. **a** appearance, **b** myocardium, **c** lung, **d** liver

with a diameter of 40 mm and a major axis of 60 mm, and the myocardium, lungs, liver, and spine were inserted in the torso parts. The myocardium was created in two different phantoms to simulate normal and defective myocardium. The left myocardium and chamber were 11 and 5 mm in diameter and 22 and 13 mm in long axis, respectively, and the myocardial wall was designed to be 3 mm in thickness. The myocardial defect was a rectangular shape (major axis: 5 mm, minor axis: 3 mm) to simulate a transmural defect, and the defective position can be set optionally. The volumes of the liver, left and right lungs were 18.4, 3.3 and 4.0 mL, respectively. The spine was created with BE-H tough bone of 1.500 g/cm^3 (KYOTO KAGAKU Co., Ltd., Kyoto, Japan) in $1 \times 1 \times 59$ mm rectangles.

Normal and inferior wall defect myocardial phantoms were filled with ^{99m}Tc and/or ^{18}F solution to simulate the SIA and DISA. The defect part was filled with non-radioactive water. The radioactive concentration of myocardium, lung, liver, and torso were 3.8, 0.8, 22.9 and 0.02 MBq/mL for ^{99m}Tc, 15.5, 2.6, 12.2 and 0.4 MBq/mL for ^{18}F, respectively. The radioactivity concentration of each organ was determined with reference to the %ID/g of Rat identified in the previous study [22]. The radioactive concentrations of ^{99m}Tc and ^{18}F for DISA were also in the same condition as the SIA.

Cylindrical phantom

The cylindrical phantom (diameter: 40 mm and length: 20 mm) was filled with ^{99m}Tc and/or ^{18}F solution to simulate the SIA and DISA. The radioactive concentration of ^{99m}Tc and ^{18}F were 4 and 16 MBq/mL, respectively. The ^{18}F/^{99m}Tc ratio with DISA was determined with reference to the radioactivity concentration ratio in the myocardial portion of the myocardial phantom.

Animal studies

Two male Wistar rats (Charles River) aged 6 weeks were used for all experiments. Our university's animal protection commission approved the experimental protocol (Approval number: AP-183950).

A normal model rat (body weight: 220 g) was injected with the ^{99m}Tc-methoxyisobutylisonitrile (MIBI) of 0.7 MBq/g through the tail vein, and the SPECT was acquired 30 min later. The next day, insulin of 8 mU/g and glucose of 1 mg/g were injected into the rats, and the blood glucose value was measured 25 min later (blood glucose level: 114 mg/dL). After 30 min of insulin and glucose administration, the ^{18}F- fluorodeoxyglucose (FDG) of 0.8 MBq/g and ^{99m}Tc-MIBI of 0.7 MBq/g were injected from the tail intravenously, and SPECT was acquired 30 min later.

A myocardial infarction model rat (body weight: 242 g) with the left coronary artery (LCA) was occluded for 20 min followed by reperfusion. Under anesthesia with 0.05 mg/kg intraperitoneal secobarbital sodium, the chest was opened to expose the heart, before a 7–0 polypropylene suture on a small-curved needle was passed under the LCA and ligated to occlude the LCA. After reperfusion, animals were allowed a week to recover before SPECT. The administration method and image timing were designed in the same protocol for normal model rats. The blood glucose value of the myocardial infarction model rat was 134 mg/dL.

Acquisition protocol and image reconstruction parameters

SPECT and PET scans were performed by the list-mode acquisition of 30 min using a VECTor$^+$/CT small-animal SPECT-PET/CT scanner equipped with a high-energy ultra-high-resolution rat and mice clustered-pinhole collimator. An energy window was centered on 511 keV $\pm$ 10% for ^{18}F and 140 keV $\pm$ 10% for ^{99m}Tc. Projection data were reconstructed by a pixel-based ordered subset expectation maximization algorithm [23]. The voxel size and subset number were set at 0.8 mm and 32 for both ^{99m}Tc and ^{18}F, and the iteration number was 8 for ^{99m}Tc and 17 for ^{18}F, respectively. A Gaussian filter with a full width at half maximum (FWHM) of 1.6 mm was applied as a post-filter. Attenuation and scatter corrections (AC and SC) were applied to the CT-based AC and triple energy window method both ^{99m}Tc and ^{18}F, whereas the spatial resolution correction was conducted for ^{18}F images only. In addition, no SC (nonSC) images were also created to validate the influence of dawnscatter from ^{18}F for DISA.

Image assessment

The uniformity of normal myocardium was evaluated by the percent coefficient of variation (%CV) using average value and standard deviation (SD) with the region of interest (ROI) on the short-axial (SA) image. The ROI was drawn on anterior, septal, inferior, and lateral myocardial walls (A) and left ventricular cavity (B) of the SA image, and the cavity contrast was calculated from average counts in ROI using Eq. 1.

$$\text{Cavity contrast} = \frac{A - B}{A} \times 100(\%) \quad (1)$$

The circumferential profile curve was drawn on the defective myocardial wall slice of the SA image, and the minimum %uptake of the defect part was calculated from the circumferential profile curve normalized by maximum counts.

The %CV of a cylindrical phantom was calculated from the mean value and SD of a 32 mm diameter (80% area) ROI on a transverse image.

Results

The %CV and cavity contrast of myocardial phantom were shown in Fig. 2. The %CVs of SIA and DISA were 19.9% and 20.7% for ^{99m}Tc with nonSC, 20.1% and 19.7% for ^{99m}Tc with SC, 22.7% and 25.7% for ^{18}F with nonSC, and 21.4% and 24.4% for ^{18}F with SC, respectively (Fig. 2A). The %CV of ^{99m}Tc SIA with nonSC was slightly lower than that of ^{99m}Tc DISA with nonSC, while the ^{99m}Tc DISA with SC showed a low %CV compared with that with nonSC. The %CV of ^{18}F with SIA was lower %CV than those with DISA. The cavity contrasts of SIA and DISA for myocardial phantom were 90.9% and 85.9% for ^{99m}Tc with nonSC, 93.4% and 89.7 for ^{99m}Tc with SC, 75.5% and 73.0% for ^{18}F with nonSC, and 81.1% and 77.8% for ^{18}F with SC, respectively (Fig. 2B). The ^{99m}Tc DISA with nonSC was lower cavity contrast than the ^{99m}Tc SIA with nonSC. While the cavity contrast of ^{18}F showed a low value compared with that of ^{99m}Tc. The minimum %uptakes of ^{99m}Tc for defect parts with SIA and DISA were 11.7% and 18.7% for nonSC, and 9.6% and 10.8% for SC, respectively. Furthermore, the minimum %uptakes of ^{18}F for defect parts with SIA and DISA were 25.3% and 25.5% for nonSC, and 21.4% and 21.7% for SC, respectively (Fig. 3). The minimum %uptake of ^{99m}Tc SIA with nonSC was a lower value compared with that of DISA, while the defect part of ^{99m}Tc DISA was equivalent to the minimum %uptake of ^{99m}Tc SIA by SC. The minimum %uptake of ^{18}F did not differ between SIA and DISA.

The vertical long axis (VLA) and SA images of normal and defective myocardium were shown in Fig. 4. The left ventricular cavity of ^{99m}Tc DISA for normal myocardium was narrowing compared with ^{99m}Tc SIA. While the left ventricular cavity of ^{18}F DISA for normal myocardium was similar compared with ^{18}F SIA. Although all defect myocardial images were visually detected clearly, the ^{99m}Tc DISA image was slightly inferior to the ^{99m}Tc SIA image in defect detectability. The defect myocardial image with ^{18}F was less visible than that with ^{99m}Tc.

The %CVs of SIA and DISA for cylindrical phantom were 3.57% and 5.06% for ^{99m}Tc with nonSC, 3.61% and 4.40% for ^{99m}Tc with SC, 7.47% and 8.31% for ^{18}F with nonSC, and 5.86% and 6.06% for ^{18}F with SC, respectively. The %CV of ^{99m}Tc SIA with nonSC was slightly lower than that of ^{99m}Tc DISA with nonSC, while the ^{99m}Tc DISA with SC showed a low %CV compared with that with nonSC. The %CV of ^{18}F SIA with nonSC was lower %CV than ^{18}F

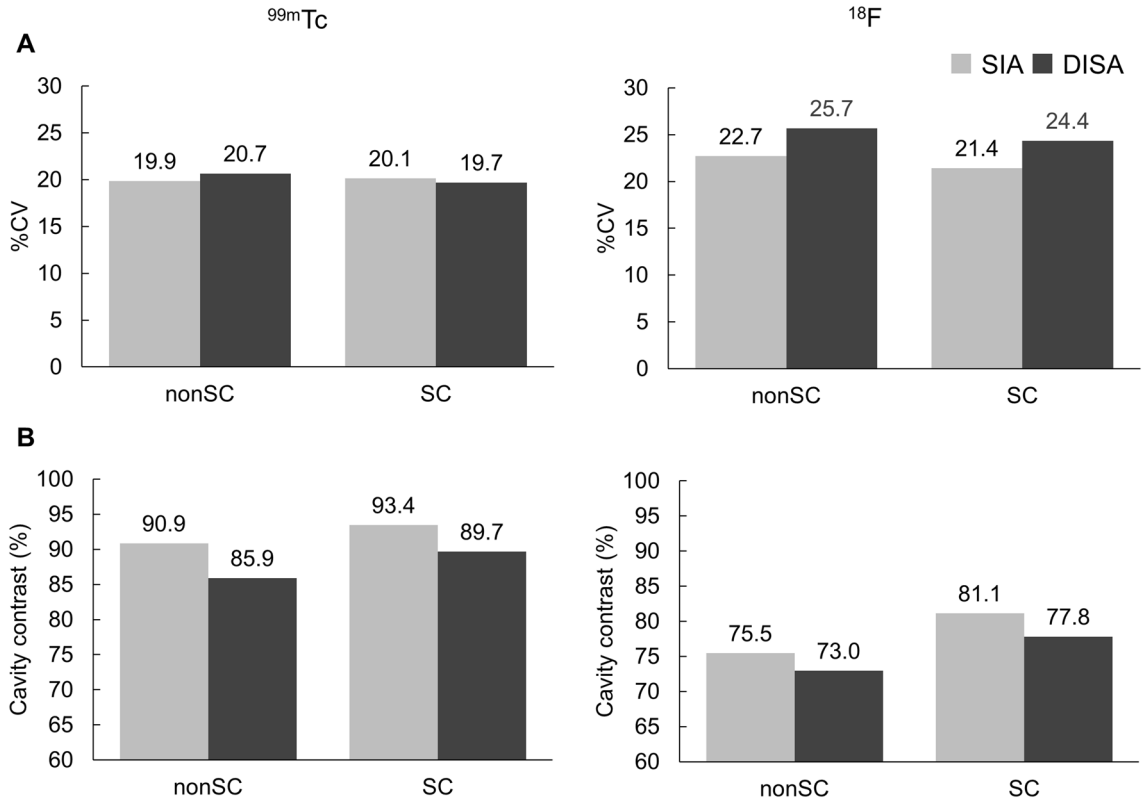

Fig. 2 The percent coefficient of variation (%CV) and cavity contrast of normal myocardium with ^{99m}Tc and ^{18}F for single-isotope acquisition (SIA) and dual-isotope simultaneous acquisition (DISA). The graph of A and B shows the %CV and cavity contrast, respectively

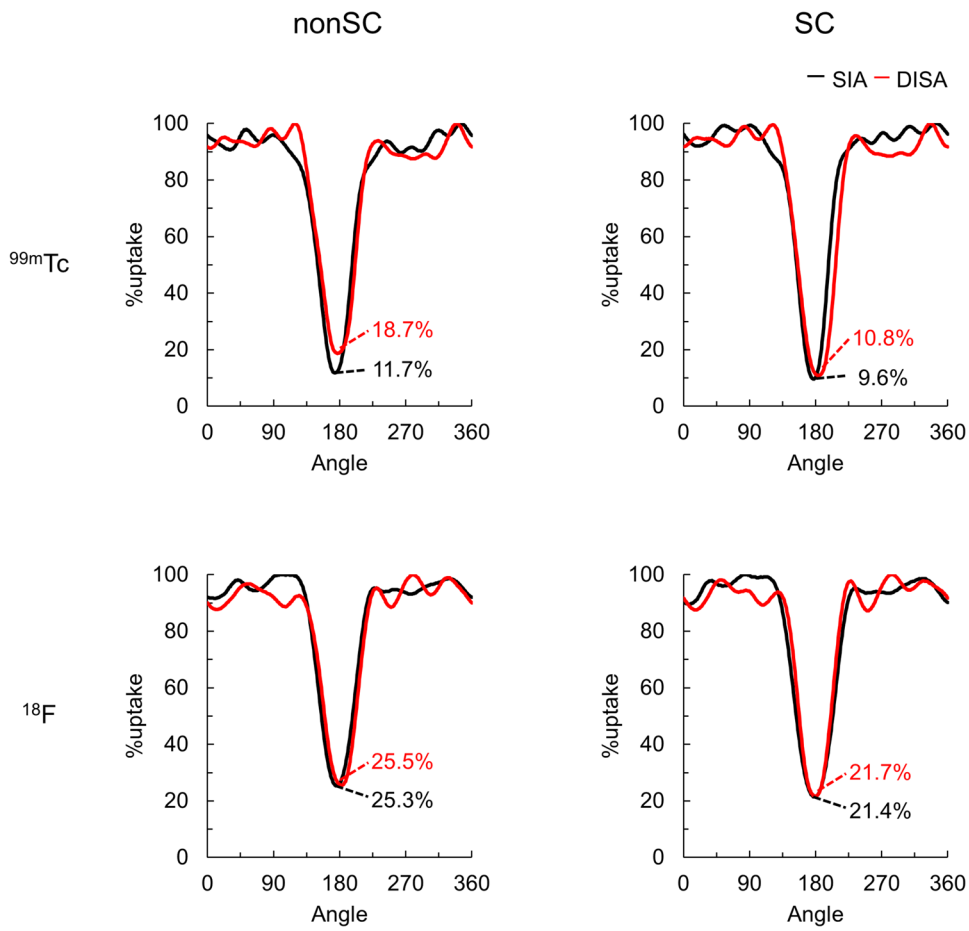

Fig. 3 Circumferential profile curve of inferior defect myocardium with ^{99m}Tc and ^{18}F for single-isotope acquisition (SIA) and dual-isotope simultaneous acquisition (DISA). The %uptake values in the graphs indicate the minimum value for each profile curve

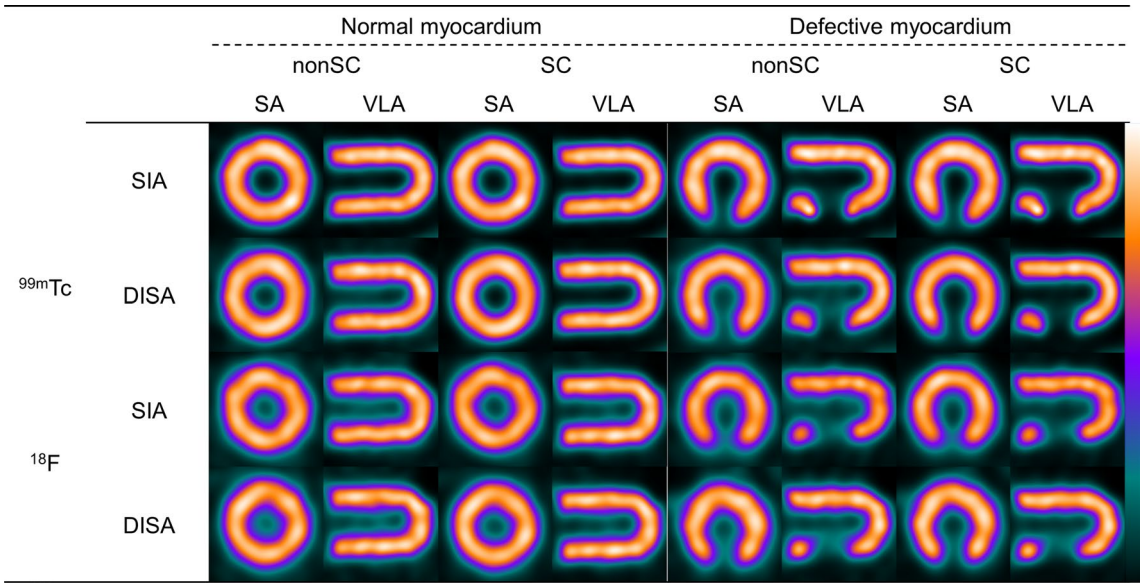

Fig. 4 Normal and defect myocardial image with ^{99m}Tc and ^{18}F for single-isotope acquisition and dual-isotope simultaneous acquisition (DISA). *SA* short-axis, *VLA* vertical long axis, *nonSC* no scatter correction, *SC* scatter correction

DISA, in addition, the %CVs of ^{18}F SIA and DISA were a low value by SC. Those trends were comparable to the %CV of the myocardial phantom.

The SA and VLA images in rats with normal and defective myocardial models were shown in Fig. 5. The cavity contrasts of SIA and DISA for a rat with the normal myocardial model were 71.7% and 65.9% for ^{99m}Tc with nonSC, 74.7% and 75.9% for ^{99m}Tc with SC, respectively. Furthermore, the cavity contrasts of nonSC and SC for ^{18}F DISA were 61.3% and 64.0%. The ^{99m}Tc DISA with nonSC image had a lower cavity contrast compared with that of ^{99m}Tc SIA with nonSC image. While the cavity contrast of ^{99m}Tc DISA with SC was visually and quantitatively equivalent to that of ^{99m}Tc SIA with SC. Furthermore, the cavity contrast showed the same tendency as the evaluation with the myocardial phantom. The defect part of a rat with the defective myocardial model were visually equivalent in ^{99m}Tc SIA and ^{99m}Tc DISA. The ^{18}F DISA image was comparable to the ^{99m}Tc DISA image in contrast and image quality.

Discussion

This study examined the ability of the novel myocardial phantom simulating the structure of a rat to demonstrate the physical phenomenon occurring in small-animal imaging. We selected SIA and DISA with ^{99m}Tc and ^{18}F in the nuclear cardiology tracers because of the advantage of the VECTor^{+}/CT SPECT-PET/CT system, which can simultaneously acquire SPECT and PET imaging [11]. Furthermore, the DISA of ^{99m}Tc and ^{18}F using VECTor^{+}/CT reported that a peak of 170 keV is generated due to the backscatter of photons interacting with the clustered-pinhole collimator of tungsten [16]. However, the previous study did not demonstrate in detail the image quality of ^{99m}Tc that was affected by the backscatter of photon from ^{18}F. Hence, we evaluated the image quality of DISA with ^{99m}Tc and ^{18}F using a novel myocardial phantom. The radioactivity concentration of the myocardium was selected to be 4, which had the highest ^{18}F/^{99m}Tc ratio in our previous study [22]. When ^{18}F/^{99m}Tc is greater than 2, the peak of 170 keV may affect the image quality of ^{99m}Tc [16]. Thus, the ^{18}F/^{99m}Tc ratio set in this study was reasonable for assessing image quality by DISA for SPECT and PET.

The ^{99m}Tc DISA with nonSC of myocardial phantom caused image inhomogeneity, low cavity contrast and poor defect detectability due to down scatter and crosstalk from the backscatter of photon, and the low image quality was improved by the SC. We evaluated image uniformity using a cylinder phantom and cavity contrast using rat images to substantiate the results shown with the myocardial phantom. Consequently, we could demonstrate that our myocardial phantom was obtained the image evaluation results comparable to another physical phantom and those of the rat.

The defect parts of ^{99m}Tc for myocardial phantom between SIA and DISA was also showed differences in image quality and %uptake affected by downscatter and crosstalk from the backscatter of photon, whereas the phenomenon could not be observed in the rat images. Rat has respiratory movement and cardiac motion, causing a blurring in the myocardial image. Hence, it was difficult to evaluate slight differences in the physical phenomenon. However, the myocardial phantom was able to reproduce the poor image quality caused by the physical phenomenon of down scatter and crosstalk from the backscatter of photon. We could demonstrate that the novel myocardial phantom is an important tool in understanding the physical phenomenon. The ^{18}F image was higher %uptake and lower contrast than the ^{99m}Tc

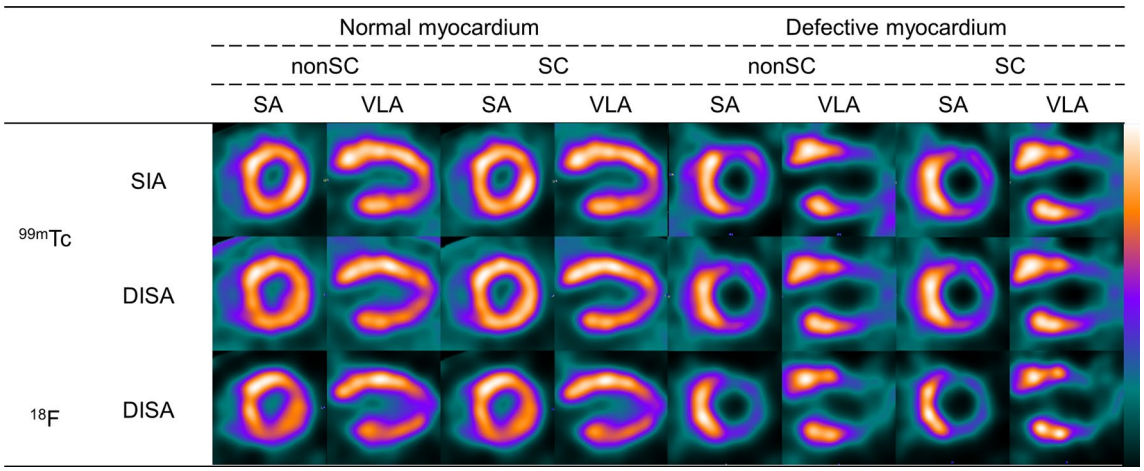

Fig. 5 Short-axis (SA) and vertical long axis (VLA) images of rat myocardium. *SIA* single-isotope acquisition, *DISA* dual-isotope simultaneous acquisition, *nonSC* no scatter correction, *SC* scatter correction

image due to a low spatial resolution. Moreover, the counting loss of ^{18}F would be caused by the lower image quality [16]. However, the ^{18}F image showed acceptable image quality thanks to the spatial resolution correction.

We evaluated the usefulness of the new myocardial phantom using DISA for ^{99m}Tc and ^{18}F, which is important for myocardial viability assessment. However, radionuclides for myocardial SPECT are available in ^{13}N, ^{123}I, and ^{201}Tl as well as ^{99m}Tc and ^{18}F. In particular, the DISA for ^{201}Tl and ^{123}I is widely used clinically [24, 25]. We would like to reveal the physical evaluation of DISA images other than ^{99m}Tc and ^{18}F using a novel myocardial phantom. In addition, we studied using a specific device that can simultaneously acquire SPECT and PET tracers. It is assumed that the new small-animal cardiac phantom can be used to evaluate the image quality of other SPECT devices, but the device dependency needs to be verified in the future.

Conclusion

We have developed a novel myocardial phantom for the rat model to evaluate the image quality for reproducing the physical phenomenon associated with radiation attenuation and scattering. Furthermore, we could demonstrate the usefulness of the novel small-animal myocardial phantom by image quality evaluation of DISA with ^{99m}Tc and ^{18}F compared with SIA. The ^{99m}Tc with SC images for DISA of ^{99m}Tc and ^{18}F were equivalent to those of SIA thanks to the improvement of defect detectability and cavity contrast by SC. Myocardial phantom studies could assist in the interpretation of quantitative analysis in small animals.

Acknowledgements We would like to thank Akira E of Hokuriku E.P., Japan for his excellent technical support of phantom production.

Funding This study was supported by JSPS KAKENHI Grant Number 18K15628.

Declarations

Conflict of interest The authors report no potential conflicts of interest relevant to this study.

References

1. Hendrikx G, Vöö S, Bauwens M, Post MJ, Mottaghy FM. SPECT and PET imaging of angiogenesis and arteriogenesis in pre-clinical models of myocardial ischemia and peripheral vascular disease. Eur J Nucl Med Mol Imaging. 2016;43(13):2433–47.
2. Berman DS, Maddahi J, Tamarappoo BK, Czernin J, Taillefer R, Udelson JE, et al. Phase II safety and clinical comparison with single-photon emission computed tomography myocardial perfusion imaging for detection of coronary artery disease: flurpiridaz F 18 positron emission tomography. J Am Coll Cardiol. 2013;61(4):469–77.
3. Yu M, Nekolla SG, Schwaiger M, Robinson SP. The next generation of cardiac positron emission tomography imaging agents: discovery of flurpiridaz F-18 for detection of coronary disease. Semin Nucl Med. 2011;41(4):305–13.
4. Dobrucki LW, Sinusas AJ. Molecular cardiovascular imaging. Curr Cardiol Rep. 2005;7(2):130–5.
5. Golestani R, Wu C, Tio RA, Zeebregts CJ, Petrov AD, Beekman FJ, et al. Small-animal SPECT and SPECT/CT: application in cardiovascular research. Eur J Nucl Med Mol Imaging. 2010;37(9):1766–77.
6. Wakabayashi H, Taki J, Inaki A, Hiromasa T, Yamase T, Akatani N, et al. Prognostic value of early evaluation of left ventricular dyssynchrony after myocardial infarction. Mol Imaging Biol. 2019;21(4):654–9.
7. Wakabayashi H, Taki J, Inaki A, Hiromasa T, Okuda K, Shibutani T, et al. Quantification of myocardial perfusion defect size in rats: comparison between quantitative perfusion SPECT and autoradiography. Mol Imaging Biol. 2018;20(4):544–50.
8. Onoguchi M, Takayama T, Tonami N, Kyogoku S, Naoi Y, Irimoto M, et al. Comparison of ^{99m}Tc-tetrofosmin uptakes on planar images with those in excised rats organs. Ann Nucl Med. 2001;15(1):33–40.
9. Han JH, Lim SY, Lee MS, Lee WW. Sodium [^{18}F] fluoride PET/CT in myocardial infarction. Mol Imaging Biol. 2015;17(2):214–21.
10. Higuchi T, Nekolla SG, Huisman MM, Reder S, Poethko T, Yu M, et al. A new ^{18}F-labeled myocardial PET tracer: myocardial uptake after permanent and transient coronary occlusion in rats. J Nucl Med. 2008;49(10):1715–22.
11. Goorden MC, van der Have F, Kreuger R, Ramakers RM, Vastenhouw B, Burbach JP, et al. VECTor: a preclinical imaging system for simultaneous submillimeter SPECT and PET. J Nucl Med. 2013;54(2):306–12.
12. Walker MD, Goorden MC, Dinelle K, Ramakers RM, Blinder S, Shirmohammad M, et al. Performance assessment of a preclinical PET scanner with pinhole collimation by comparison to a coincidence-based small-animal PET scanner. J Nucl Med. 2014;55(8):1368–74.
13. Magota K, Kubo N, Kuge Y, Nishijima K, Zhao S, Tamaki N. Performance characterization of the Inveon preclinical small-animal PET/SPECT/CT system for multimodality imaging. Eur J Nucl Med Mol Imaging. 2011;38(4):742–52.
14. Spinks TJ, Karia D, Leach MO, Flux G. Quantitative PET and SPECT performance characteristics of the Albira Trimodal preclinical tomograph. Phys Med Biol. 2014;59(3):715–31.
15. Hoffmann JV, Janssen JP, Kanno T, Shibutani T, Onoguchi M, Lapa C, et al. Performance evaluation of fifth-generation ultra-high-resolution SPECT system with two stationary detectors and multi-pinhole imaging. EJNMMI Phys. 2020;7(1):64.
16. Miwa K, Inubushi M, Takeuchi Y, Katafuchi T, Koizumi M, Saga T, et al. Performance characteristics of a novel clustered multi-pinhole technology for simultaneous high-resolution SPECT/PET. Ann Nucl Med. 2015;29(5):460–6.
17. Takahashi Y, Mochiki M, Koyama K, Ino T, Yamaji H, Kawakami A. Evaluation of simultaneous dual-radioisotope SPECT imaging using (18)F-fluorodeoxyglucose and (99m)Tc-tetrofosmin. Asia Ocean J Nucl Med Biol. 2016;4(2):66–71.
18. Slart RH, Bax JJ, van Veldhuisen DJ, van der Wall EE, Irwan R, Sluiter WJ, et al. Prediction of functional recovery after revascularization in patients with chronic ischaemic left ventricular dysfunction: head-to-head comparison between ^{99m}Tc-sestamibi/^{18}F-FDG DISA SPECT and ^{13}N-ammonia/ ^{18}F-FDG PET. Eur J Nucl Med Mol Imaging. 2006;33(6):716–23.
19. Kobayashi M, Matsunari I, Nishi K, Mizutani A, Miyazaki Y, Ogai K, et al. Simultaneous acquisition of (99m)Tc- and (123)

I-labeled radiotracers using a preclinical SPECT scanner with CZT detectors. Ann Nucl Med. 2016;30(4):263–71.
20. Johnson LC, Guerraty MA, Moore SC, Metzler SD. Quantification of myocardial uptake rate constants in dynamic small-animal SPECT using a cardiac phantom. Phys Med Biol. 2019;64(6): 065018.
21. Branderhorst W, Vastenhouw B, van der Have F, Blezer EL, Bleeker WK, Beekman FJ. Targeted multi-pinhole SPECT. Eur J Nucl Med Mol Imaging. 2011;38(3):552–61.
22. Horikawa Y, Onoguchi M, Shibutani T, Kanno T, Mochizuki T, Shiba K. Organ uptake ratio using a small animal SPECT-PET/CT system - comparison with organs removed by rats. Jpn J Nucl Med Technol. 2019;39(suppl):377.
23. Branderhorst W, Vastenhouw B, Beekman FJ. Pixel-based subsets for rapid multi-pinhole SPECT reconstruction. Phys Med Biol. 2010;55(7):2023–34.
24. Momose M, Fukushima K, Kondo C, Serizawa N, Suzuki A, Abe K, et al. Diagnosis and detection of myocardial injury in active cardiac sarcoidosis-significance of myocardial fatty acid metabolism and myocardial perfusion mismatch. Circ J. 2015;79(12):2669–76.
25. Maruyama Y, Masaki N, Shimizu Y, Honda N, Yoshimoto N. Correlation of left ventricular dyssynchrony with myocardial stunning using dual single photon emission computed tomography of ^{123}iodine-beta-methyl iodophenyl pentadecanoic acid and ^{201}thallium scintigraphy after reperfusion therapy. Ann Nucl Med. 2009;23(9):799–805.